Open Research Online

Atomistic and *ab initio* DFT modelling of the defect structures in Al³⁺/Cr³⁺-doped and co-doped Y₃Fe₅O₁₂

Journal Item

oro.open.ac.uk

Atomistic and *ab initio* DFT modelling of the defect structures in Al^{3+}/Cr^{3+}-doped and co-doped $Y_3Fe_5O_{12}$

Hisham. M. Widatallah[1] , Muataz S. Al-Barwani[2], Elaine. A. Moore[3], Mohamed E. Elzain[1]

[1]Physics Department, Sultan Qaboos University, Al-Khoudh, Muscat 123, Oman.
[2]High Performance Computing Center, New York University, Abu Dhabhi, U.A.E.
[3]Department of Life, Health, and Chemical Sciences, Open University, Walton Hall, Milton Keynes, MK7 6AA, UK.

Abstract

The defect structures when $Y_3Fe_5O_{12}$ is doped with either Al^{3+} or Cr^{3+}, and evenly co-doped with both, which have been a matter of controversy in the literature, are modelled using atomistic and *ab initio* DFT methods. When $Y_3Fe_5O_{12}$ is doped with Al^{3+}, the defect reaction energy obtained marginally favors the preferential substitution of Al^{3+} for Fe^{3+} at the tetrahedral sites as opposed to octahedral ones. This is indicative that for Al^{3+}-doped samples processed at elevated temperatures, or containing undetected impurities, the substitution of Al^{3+} for octahedral Fe^{3+} is likely. To model the defect structure of the Cr^{3+} - doped $Y_3Fe_5O_{12}$, it was essential that the Cr^{3+} ions crystal field stabilization energy (CFSE) and the Fe^{3+}-O^{2-}- Cr^{3+} spin-spin coupling derived from the *ab initio* DFT calculations ,be taken into account. The results show the substitution of the Cr^{3+} ion for an octahedral Fe^{3+} ion to be energetically favorable relative to its substitution for a tetrahedral Fe^{3+} one. It is also shown that the antisite defect, where the Cr^{3+} ion substitutes for Y^{3+} at a dodecahedral site with the expelled Y^{3+} ion substituting for an octahedral Fe^{3+} ion, is possible under certain processing conditions. For the Al^{3+} /Cr^{3+} co-doped $Y_3Fe_5O_{12}$, the Al^{3+} and Cr^{3+} ions were found to, respectively, substitute for the tetrahedral and octahedral Fe^{3+} ions. The energy values obtained suggest this defect structure to be insensitive to the processing conditions and/or the presence of undetected impurities. The structural and magnetic implications of these defect structures are discussed.

1 Introduction

Yttrium iron garnet (YIG) of the composition $Y_3Fe_5O_{12}$ is an attractive material that has been extensively used in areas such as telecommunication, microwave and magneto-optical recording industries [1,2]. Figure 1 shows the compound to have bcc unit cell (space group $Ia\bar{3}d$; *no. 230*) where the Y^{3+} ions reside at the dodecahedral (24c) sites, 2/5 of the Fe^{3+} ions occupy the octahedral (16a) sites and the remaining Fe^{3+} ions occupy the tetrahedral (24d) sites

in the O^{-2} sublattice [4,5]. The compositional formula is adequately represented as $\{Y_3\}[Fe_2^{3+}]_{(a)}(Fe_3^{3+})_{(d)}O_{12}$ where the brackets refer to dodecahedral, octahedral (*a*) and tetrahedral (*d*) sites respectively.

Figure 1 about here

The physical and chemical properties that YIG exhibits are closely related to its crystal structure. YIG is ferrimagnetic with the spins of the *Fe³⁺* cations at the octahedral and tetrahedral sublattices aligned in opposite directions. Hence the magnetization can be varied by substituting the Fe^{3+} cations the solid with magnetic/diamgnetic ones [3-5]. Consequently, determining the crystal defect structure of cation-doped YIG compounds is of crucial importance in understanding the material's behavior. While both experimental and theoretical investigations show the location of the doped cations within the YIG structure to largely depend on their sizes [6], there exist controversial lieterature reports regarding site preferences of some substituted cations. For example, Gilleo and Geller [7] and Kim et al [8], using experimentally derived data, argue that the substituted *Al³⁺* ions exclusively substitute the Fe^{3+} at the *tetrahedral d*-sites leading to a lower magnetization relative to that of pure YIG. Their proposed cation distribution *viz.* $\{Y_3\}[Fe_2^{3+}]_a(Fe_{3-x}^{3+}Al_x^{3+})_dO_{12}$ is at variance with that deduced from an atomistic simulation study [9] where the *Al³⁺* ions are predicted to substitute for Fe^{3+} at the *octahedral a*-sites implying a cation distribution of the type $\{Y_3\}[Fe_{2-x}^{3+}Al_x^{3+}]_a(Fe_3^{3+})_dO_{12}$. Studies based on magnetic measurements and atomistic simulations suggest for Cr³⁺-doped YIG a cationic distribution of the form $\{Y_3\}[Fe_{2-x}^{3+}Cr_x^{3+}]_a(Fe_3^{3+})_dO_{12}$ where the Cr³⁺ ions exclusively substitute Fe³⁺ ions at the octahedral *a*-sites in [6,9,10]. However, the same magnetic data [e.g. see 6,10], may equally be interpreted assuming the Cr³⁺ ions to occupy *interstitial* octahedral sites balanced by octahedral Fe³⁺ vacancies rather than the mere substitution of octahedral Fe³⁺ by Cr³⁺ [6,9,10].

The positions of the Al³⁺ and Cr³⁺ ions in the structure of co-doped Y*₃*Fe*₅₋₂ₓ*Al*ₓ*Cr*ₓ*O*₁₂*, have, also, been reported and the experimentally deduced cationic distribution is also a matter of controversy [12-15]. For instance Murumkar et al concluded from Mössbauer spectroscopic measurements on Y*₃*Fe*₅₋₂ₓ*Al*ₓ*Cr*ₓ*O*₁₂* that while the Al³⁺ impurity ions exclusively substitute Fe³⁺ at the octahedral sites, the Cr³⁺ ions substitute at both octahedral and tetrahedral sites [12]. This

to be contrasted with an earlier study where the results of magnetic measurements were assumed to be a consequence of the substitution of nearly all Cr^{3+} and 3/5 of all Al^{3+} ions in $Y_3Fe_{5-2x}Al_xCr_xO_{12}$ for tetrahedral Fe^{3+} ions with the remaining Al^{3+} substituting octahedral Fe^{3+} [13]. A different defect structure model was proposed using Mössbauer spectroscopy with both Al^{3+} and Cr^{3+} ions only replacing octahedral Fe^{3+} in the co-doped YIG [14]. In a relatively recent study of $Y_3Fe_{5-2x}Al_xCr_xO_{12}$, Bouziane et al using magnetic and Mössbauer spectroscopic measurements have concluded that Cr^{3+} substitutes for octahedral Fe^{3+} whilst Al^{3+} replaces Fe^{3+} at the tetrahedral sites [15]. The latter cation distribution was justified mainly on structural grounds by noting that smaller lattice parameter of the doped compound could be associated with the smaller tetrahedral ionic radius of Al^{3+} ion relative to that of the substituted Fe^{3+} [16].

Atomistic simulations are increasingly emerging as a powerful tool to optimize and determine defect structures in various inorganic oxides where the interactions between ions can adequately be described by parameterized pairwise potentials [9,17-25]. The method has enabled the prediction of defect structures based on ionic size, charge and compensation mechanisms in numerous complex oxide materials including $Y_3Al_5O_{12}$ [20], lithiated Ti-doped α-Fe_2O_3 [20], $Li_{0.5}Fe_{2.5}O_4$ [22,23], Sb_2O_4 [24], and La_2CuO_4 [25]. In all these studies semi-empirical interatomic potentials were used to predict the cation distribution within the material's anionic crystalline network using a periodic cell to represent the infinite ideal crystal. The output values of input physical properties give a measure of the quality of the simulation when compared with their experimentally-determined counterparts..

In the present paper, we investigate afresh the cationic site-preference in Al^{3+}- and Cr^{3+}-doped and co-doped YIG using systematic interatomic potential calculations to determine the most energetically favorable sites for Al^{3+} in $Y_3Al_xFe_{5-x}O_{12}$, Cr^{3+} in $Y_3Cr_xFe_{5-x}O_{12}$ and both Al^{3+} and Cr^{3+} in $Y_3Al_xCr_xFe_{5-2x}O_{12}$ with low concentrations of the doped ions. The role played by the spin-spin coupling in determining the site of magnetic Cr^{3+} impurity was further investigated with quantum mechanical *ab initio* calculations. The results show the Al^{3+} ions in $Y_3Al_xFe_{5-x}O_{12}$ to preferentially substitute for Fe^{3+} at the tetrahedral sites whereas the Cr^{3+} ions preferentially substitute for octahedral Fe^{3+} in $Y_3Cr_xFe_{5-x}O_{12}$. For $Y_3Al_xCr_xFe_{5-2x}O_{12}$, the Al^{3+} the Cr^{3+} and Al^{3+} ions were found to substitute for octahedral and tetrahedral Fe^{3+} ones respectively. The structural and magnetic implications of the proposed defect structures are discussed in the light of reported data on Al^{3+} and Cr^{3+}- substituted and co-substituted YIGs. The computational

methods used are presented in section 2. We first start by describing how atomistic simulations were used to determine the defect structures for the Al^{3+}- and Cr^{3+} -doped and co-doped YIG compounds. This will be followed by describing the ab initio approach used. In section 3 we present the results and discuss them to find the energetically most favourable defect structures. Conclusions are given in section 4.

2.Computational methods:

2.1. Atomistic Simulation:

Inter-atomic potential calculations were carried out using the program GULP (Version 4.0) [24] in which the force field used consists of a pairwise interaction energy that is composed of a Buckingham potential to model the short-range Pauli repulsion and the leading term of any dispersion energy and the Coulomb interaction, such that the interatomic potential V_{ij} is

$$V_{ij} = A \exp(-r_{ij}/\rho) - C r_{ij}^{-6} + q_i q_j / r_{ij} \qquad (1)$$

where A, ρ and C are empirical constants, q is the charge of the ionic species and r_{ij} the inter-ionic spacing. The electronic polarizability of the ions in the crystal is introduced by means of the shell model [18]. Consequently, the ions are described as consisting of an ionic core (charge X) to which the shell valance electrons (charge Y) is coupled via an isotropic harmonic restoring force of spring constant k. The total ionic charge is $q = X + Y$ and the free electron polarizability is $\alpha = Y^2/k$ [18]. GULP uses the Mott–Littleton approach to point defect calculation with the crystal surrounding the defect divided into three spherical regions. In the first region, all the ions are treated exactly and are allowed to relax their positions in response to the defect. The radius of this region was taken to be 6 Å. In the second region, whose radius was taken to be 12 Å, the individual ions are displaced. The ions in a harmonic potential well presumably approximate the response to the electrostatic force of the defect. A similar assumption is made for the third region, but only polarization of sub-lattices is considered. The inter-atomic potential parameters shown in Table 1 for O^{2-}-O^{2-}, Y^{3+}-O^{2-}, $Fe^{3+}_{(a)}$-O^{2-} and $Fe^{3+}_{(d)}O^{2-}$ were derived by emprical fitting to the properties of $Y_3Fe_5O_{12}$ [18]. The A and ρ potential parameters for the O^{2-}–O^{2-} interaction [18] are identical to those in ref. [17], and we, therefore, have used the Al^{3+}–O^{2-} and Cr^{3+}–O^{2-} parameters given there. The C value parameter for the O^{2-}–O^{2-} interaction was taken from the
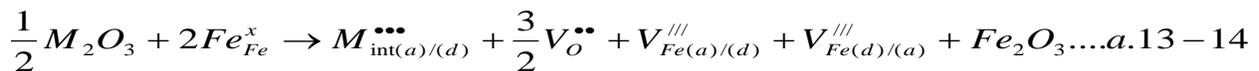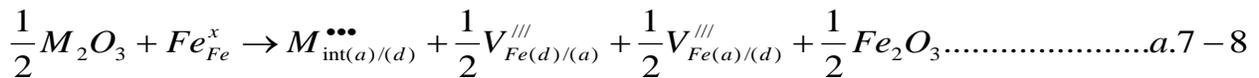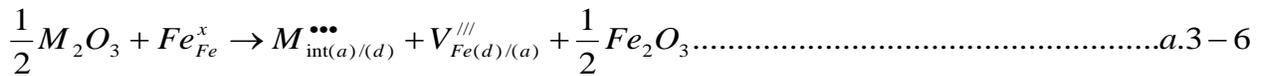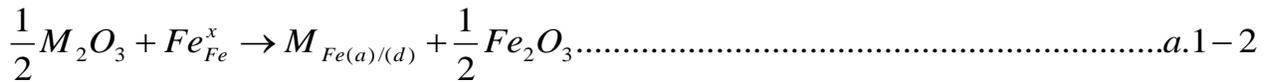
parameter set obtained by Donneberg and Catlow by transferring empirical shell parameters from Y_2O_3 and α-Fe_2O_3 for $Y_3Fe_5O_{12}$ [18].
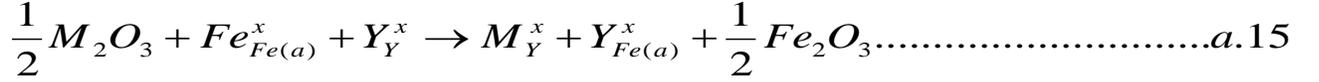
Table 1 about here

As Al^{3+} and Cr^{3+} ions are the minority species, we considered models for the defect structure in which these ions are present as point defects (substitutional or interstitial impurities) in $\{Y_3\}[Fe_2^{3+}]_a(Fe_3^{3+})_dO_{12}$. We stress that in addition to the models in which the dopant Al^{3+} (or Cr^{3+}) ions substitute for Fe^{3+} at the octahedral and tetrahedral sites that were considered in the atomistic simulation study of Donnerberg and Catlow [9], we consider a multitude of possible defect structures that, to our knowledge, have not been considered previously. Specifically the occupation of the dopant ions for interstitial sites was considered. Vacancies of Fe^{3+} and O^{2-} are assumed to the balancing defects. Reduction of Fe^{3+} to Fe^{2+} was not considered as there is no experimental support for it as was the substitution for Y^{3+} by either Cr^{3+} or Al^{3+}. Noting that Donner and Catlow [18] predict the presence of Y/Fe antisite intrinsic defects in $Y_3Fe_5O_{12}$, we have explored the possibility that the Al^{3+} or Cr^{3+} ions substituting for Fe^{3+} on Y^{3+} sites with the expelled Y^{3+} ion replacing Fe^{3+} at an octahedral site. The present study, to the best of our knowledge, is first theoretical study on the defect structures in Al^{3+}/Cr^{3+}-*co-doped* YIG.

. Below, and using Kröger-Vink notation, we present all possible defect reactions considered in the present study for atomistic simulations. It is worth noting that some of these defect reactions were reported experimentally to be the most favorable as mentioned above. The octahedral and tetrahedral sites are referred with the subscripts (*d*) and (*a*) respectively.

(i) *Defect reactions for M-substituted YIG ($Y_3M_xFe_{5-x}O_{12}$); (M=Al or Cr):*

$$\frac{1}{2}M_2O_3 + Fe_{Fe}^x \rightarrow M_{Fe(a)/(d)} + \frac{1}{2}Fe_2O_3 \dots\dots\dots\dots\dots\dots\dots\dots\dots\dots\dots\dots\dots\dots\dots a.1-2$$

$$\frac{1}{2}M_2O_3 + Fe_{Fe}^x \rightarrow M_{int(a)/(d)}^{\bullet\bullet\bullet} + V_{Fe(d)/(a)}^{'''} + \frac{1}{2}Fe_2O_3 \dots\dots\dots\dots\dots\dots\dots\dots\dots\dots a.3-6$$

$$\frac{1}{2}M_2O_3 + Fe_{Fe}^x \rightarrow M_{int(a)/(d)}^{\bullet\bullet\bullet} + \frac{1}{2}V_{Fe(d)/(a)}^{'''} + \frac{1}{2}V_{Fe(a)/(d)}^{'''} + \frac{1}{2}Fe_2O_3 \dots\dots\dots\dots a.7-8$$

$$\frac{1}{2}M_2O_3 + 2Fe_{Fe}^x \rightarrow M_{int(a)/(d)}^{\bullet\bullet\bullet} + \frac{3}{2}V_O^{\bullet\bullet} + 2V_{Fe(a)/(d)}^{'''} + Fe_2O_3 \dots\dots\dots\dots\dots a.9-12$$

$$\frac{1}{2}M_2O_3 + 2Fe_{Fe}^x \rightarrow M_{int(a)/(d)}^{\bullet\bullet\bullet} + \frac{3}{2}V_O^{\bullet\bullet} + V_{Fe(a)/(d)}^{'''} + V_{Fe(d)/(a)}^{'''} + Fe_2O_3 \dots a.13-14$$

5

$$\frac{1}{2}M_2O_3 + Fe^x_{Fe(a)} + Y^x_Y \rightarrow M^x_Y + Y^x_{Fe(a)} + \frac{1}{2}Fe_2O_3 \dots\dots\dots\dots\dots\dots a.15$$

(ii) *Defect reactions for Al^{3+} and Cr^{3+} co-substituted YIG ($Y_3Al_xCr_xFe_{5-2x}O_{12}$):*

$$\frac{1}{4}Al_2O_3 + \frac{1}{4}Cr_2O_3 + Fe^x_{Fe} \rightarrow \frac{1}{2}Al_{Fe(a)/(d)} + \frac{1}{2}Cr_{Fe(a)/(d)} + \frac{1}{2}Fe_2O_3 \dots\dots\dots\dots b.1-4$$

$$\frac{1}{4}Al_2O_3 + \frac{1}{4}Cr_2O_3 + Fe^x_{Fe} \rightarrow Cr^{\bullet\bullet\bullet}/Al^{\bullet\bullet\bullet}_{int(a)/(d)}) \frac{1}{2}Cr/Al_{Fe(d)/(a)} + \frac{1}{2}V'''_{Fe(a)/(d)} + \frac{1}{2}Fe_2O_3 \dots\dots\dots\dots b.5-20$$

$$\frac{1}{4}Al_2O_3 + \frac{1}{4}Cr_2O_3 + Fe^x_{Fe} \rightarrow \frac{1}{2}Cr^{\bullet\bullet\bullet}_{int(a)/(d)} + \frac{1}{2}Al^{\bullet\bullet\bullet}_{int(a)/(d)} + V'''_{Fe(a)/(d)} + \frac{1}{2}Fe_2O_3 \dots\dots\dots b.21-24$$

$$\frac{1}{4}Al_2O_3 + \frac{1}{4}Cr_2O_3 + Fe^x_{Fe} \rightarrow \frac{1}{2}Cr^{\bullet\bullet\bullet}_{int(a)/(d)} + \frac{1}{2}Al^{\bullet\bullet\bullet}_{int(a)/(d)} + \frac{1}{2}V'''_{Fe(d)} + \frac{1}{2}V'''_{Fe(a)} + \frac{1}{2}Fe_2O_3 \dots\dots b.25-28$$

$$\frac{1}{4}Al_2O_3 + \frac{1}{4}Cr_2O_3 + Fe^x_{Fe} \rightarrow \frac{1}{2}Cr^{\bullet\bullet\bullet}_{int(a)/(d)} + \frac{1}{2}Al^{\bullet\bullet\bullet}_{int(a)/(d)} + \frac{3}{2}V^{\bullet\bullet}_O + 2'''_{Fe(a)/(d)} + Fe_2O_3 \dots\dots\dots b.29-36$$

$$\frac{1}{4}Al_2O_3 + \frac{1}{4}Cr_2O_3 + Fe^x_{Fe} \rightarrow \frac{1}{2}Cr^{\bullet\bullet\bullet}_{int(a)/(d)} + \frac{1}{2}Al^{\bullet\bullet\bullet}_{int(a)/(d)} + \frac{3}{2}V^{\bullet\bullet}_O + V'''_{Fe(a)} + V'''_{Fe(d)} + Fe_2O_3 \dots\dots b.37-40$$

$$\frac{1}{4}Al_2O_3 + \frac{1}{4}Cr_2O_3 + \frac{1}{2}Fe^x_{Fe(a)} + \frac{1}{2}Fe^x_{Fe(d)} + \frac{1}{2}Y^x_Y \rightarrow \frac{1}{2}Cr_Y + \frac{1}{2}Al^x_{Fe(d)} + \frac{1}{2}Y^x_{Fe(a)} + \frac{1}{2}Fe_2O_3 \dots\dots b.41$$

2.2. Ab initio DFT calculations

Single point *ab initio* Density functional theory (DFT) calculations were carried out for the cases that involved doping with the magnetic ions Cr^{3+} using the CRYSTAL09 code which is a periodic quantum-mechanical *ab initio* code for calculating the total-energy-dependent and wave-function-dependent properties of crystalline solids [26,27]. This code is based on the *ab initio* periodic linear combination of atomic orbitals (LCAO) methods. Becke's three-parameter Lee–Yang–Parr (B3LYP) Hamiltonian, which contains a hybrid DFT exchange-correlation term has been used [28,29]. The localized gaussian-type all-electron basis sets used were Y^{3+} 976631(3d,d) [30], Fe^{3+} 86411(4d,d) [31], Al^{3+} 8511(d)[32], Cr^{3+} 86411(4d,d) [33] and O^{2-} 8411 [29]. The cell parameter for cubic $Y_3Fe_5O_{12}$ was taken as 12.3563 Å [34]. The ions were placed on the ideal fractional positions of $Y_3Fe_5O_{12}$. Models with 1-3 Cr^{3+} ions substituting for Fe^{3+} at the (*a*) and/or (*d*) sites per unit cell, and with one Al^{3+} and one Cr^{3+} on (*a*) and/or (*d*) sites were studied. The spins on the Cr^{3+} ions were set to be either parallel or anti-parallel to the Fe^{3+} spins on the same type of position. The magnetic structure was analyzed using Mulliken atomic charges.

3. Results and discussion:

3.1. Defect structures of $Y_3Al_xFe_{5-x}O_{12}$ and $Y_3Cr_xFe_{5-x}O_{12}$

Using the interatomic potential parameters given in Table 1, the calculated lattice energies of α-Fe_2O_3, Al_2O_3 and Cr_2O_3 and the energies of the point defects considered in the $Y_3Fe_5O_{12}$ structure are given in Table 2. The calculated point defect energies, required to calculate the energies of the defect reactions where the dopant ions substitutes for Fe^{3+} ions at octahedral and tetrahedral sites, slightly differ from those given by Donnerberg and Catlow [9] even though similar potential parameters were used in both studies. This could stem from a slight difference between the value of the lattice parameter used in our simulation (12.376 Å [15]) and that used in [9] which was not given. Another reason could be the different radii of the Mott-Littleton regions used in both studies. Specifically in [9] the radius of region 1 was 8.7 Å, whereas in the present study that region was divided into two with radii of 6 Å and 12 Å as explained in 2.1.

The energies given in Table 2 were then used to calculate the energies of the defect reactions (*a*.1-15) considered for the Al^{3+}- or Cr^{3+}-doped $Y_3Fe_5O_{12}$ compounds of the composition $Y_3Al_xFe_{5-x}O_{12}$ and $Y_3Cr_xFe_{5-x}O_{12}$ as shown in Table 3. Clearly defect reactions involving simple substitution of Al^{3+} (Cr^{3+}) ions for Fe^{3+} ions at the octahedral and tetrahedral sites (*a*.1 and *a*.2) are energetically favorable relative to those involving occupation of interstitial sites (*a*.3-14). Accordingly we exclude the occupation of interstitial sites in the YIG structure by the Al^{3+} or Cr^{3+} ions.

Table 2 about here

Table 3 about here

The results indicate a preference by the dopant ion Al^{3+}(Cr^{3+}) for the tetrahedral sites (a.2), as opposed to octahedral ones (*a*.1). While this is consistent with the conclusion derived on the basis of the lower magnetization of $Y_3Al_xFe_{5-x}O_{12}$ relative to that of pure $Y_3Fe_5O_{12}$ [7,8], it is at variance with conclusions derived on the basis of atomistic simulations where the Al^{3+} ions were predicted to substitute for the octahedral Fe^{3+} ions [9]. Furthermore reaction (*a*.2) with the Cr^{3+} ion substituting for tetrahedral Fe^{3+} cannot explain the observed higher magnetisation of $Y_3Cr_xFe_{5-x}O_{12}$ relative to that of $Y_3Fe_5O_{12}$ [6,10], which according to the Neél's two sub-lattice model is explicable in terms of the substitution of Cr^{3+} ions for octahedral Fe^{3+} ones. It is also

incompatible with the inference that the Cr^{3+} ions exclusively substitute for the octahedral Fe^{3+} ions using atomistic simulations [9].

To understand the origin of these conflicting defect structure models, one notes (Table 3) that the energy associated with the substitution of Al^{3+} for tetrahedral Fe^{3+} (*a*.2) is only 0.5 eV more favorable than that with Al^{3+} substituting for an octahedral Fe^{3+} ion (*a*.1). It is pertinent to note that Cr^{3+}, unlike Al^{3+}, being a high spin d^3 transition metal ion will be stabilized on the octahedral sites by virtue of the crystal field stabilisation energy (CFSE) [11]. Indeed the energy difference between defect model with the Cr^{3+}-substituting for tetrahedral Fe^{3+} (a.2) and that when it substitutes for octahedral Fe^{3+} (*a*.1) becomes very small if we take into account the CFSE which for Cr^{3+} ions on octahedral sites in minerals has been estimated from spectroscopic studies to be ~ 2.6 eV [11]. Allowing for the smaller crystal field splitting in tetrahedral environments (t) relative to octahedral ones (o), viz. $\Delta_t \approx 4/9 \ \Delta_o$, and the different electronic configurations of Fe^{3+} and Cr^{3+}, we estimate the CFSE for Cr^{3+} on a tetrahedral site to be 0.77 eV. This would make the defect energies for the substitution of Cr^{3+} for Fe^{3+} on tetrahedral and octahedral sites -3.36 and -3.0 eV respectively. This still favors tetrahedral substitution but by a reduced amount of energy relative to that calculated in Table 3. Such small differences between the reaction energies associated with the defect reaction models *a*.1 and *a*.2 are implicative of the sensitivity of the defect structure of the Cr^{3+}-substituted $Y_3Fe_5O_{12}$ to the preparation routes as well as the presence of undetected impurities in the initial reactants. So while the exclusive substitution of the tetrahedral Fe^{3+} ions by the Cr^{3+} ones implies a lower magnetization of the relative to that of the pure compound, it is possible for samples prepared at very high temperatures that the substitution takes place at the octahedral sites leading to a slight increase in the magnetization as has been reported [6,10]. Also mentioned earlier in the case of Al^{3+}, the presence of any unknown point defects in the initial precursors may lead the Cr^{3+} ions to substitute octahedral Fe^{3+} rather than tetrahedral Fe^{3+} ones as proposed by experimentally [6,9,10].

A further factor which may play a role in the distribution of the cations and defects in $Y_3Cr_xFe_{5-x}O_{12}$ which contains the different magnetic ions Fe^{3+} and Cr^{3+} at sites with different O^{2-} coordination is spin-spin interactions. To investigate this we carried out the DFT calculations using the basis sets described in section 2.2 to study the ferromagnetic and antiferromagnetic coupling when the Cr^{3+} ions substitute for Fe^{3+} at the tetrahedral and octahedral sites. The results

8

showed that the difference in energy between the states in which the Cr^{3+} spins ferromagnetically couple with those of Fe^{3+} and antiferromagnetically couple with them is much smaller when the Cr^{3+} ions substitute at tetrahedral sites (0.00819 eV per formula unit) than when they substitute at the octahedral sites (0.0525 eV per formula unit). This implies that Fe^{3+}-O^{2-}-Cr^{3+} spin-spin coupling is weaker between ions on tetrahedral sites and that Cr^{3+} ions on these sites could be randomly spin-oriented at high temperatures in particular for substitution on tetrahedral sites (kT = 0.0256 eV at 298 K) and thus have an effect on the magnetization equivalent to that of a non-magnetic ion such as Al^{3+}. This would lower the magnetic moment below that expected for substitution of Cr^{3+} on tetrahedral Fe^{3+} sites following Neél's assumption that all spins in the tetrahedral sub-lattice couple ferromagnetically. The increased magnetization reported in experimental studies of on $Y_3Cr_xFe_{5-x}O_{12}$ [6,10] is, thus, consistent with the substitution of the Cr^{3+} ions for Fe^{3+} at the octahedral sites. The magnetic moments (Mulliken α - β) were found to be higher for Fe^{3+} on the octahedral sites – 4.25 as opposed to 4.09 on the tetrahedral sites. For Cr^{3+} the reverse was true – 2.92 on the octahedral sites but 3.01 on the tetrahedral sites. Substitution on an octahedral site was found to be more favourable than on a tetrahedral site for both Cr^{3+} and Al^{3+}. However relaxation of the structure in the surroundings of these ions could alter this conclusion. Substituting Cr^{3+} onto the octahedral site and Al^{3+} on the tetrahedral site was found to be 0.00446 eV per formula unit more favourable than the reverse. Again, however this ignores relaxation of the structure.

Let us consider the antisite defect reaction (a.15) where the impurity Al^{3+}(Cr^{3+}) substitutes for a Y^{3+} at the dodecahedral sites with the concomitant substitution of the expelled Y^{3+} for an adjacent octahedral Fe^3. The energies obtained for this defect model were 1.57 eV for Al^{3+} and -0.54 eV for Cr^{3+} and are both higher than those obtained for the simple substitution by either ion for tetrahedral Fe^{3+} (a.2). It is interesting to note that when substituting with Cr^{3+} the antisite defect energy (a.15), viz. -0.54 eV, is lower than that when Cr^{3+} simply substitutes for an octahedral Fe^{3+}, namely -0.40 eV, (a.1). So as proposed above, for $Y_3Cr_xFe_{5-x}O_{12}$ processed at high temperature or produced from reagents with undetected point defects not only the substitution of octahedral Fe^{3+} ions by Cr^{3+} ions is possible, but substitution of Y^{3+} at the dodecahedral sites by the Cr^{3+} ions with the expelled Y^{3+} ion substituting Fe^{3+} at octahedral sites. In exploring this antisite defect structure (a.15), we note that despite the increase in metal-oxygen distance when the larger Y^{3+} ion (104 pm) substituted for the smaller octahedral Fe^{3+} ion

(79 pm) [16], the site remained approximately octahedral as is shown in Figure 2. This is to be contrasted with the effect of substituting the smaller Cr^{3+} ion for the larger Y^{3+} on the dodecahedral site which led to a considerable distortion of that site as shown in Figure 3 (a). It is seen that the Cr^{3+} ion is located off-centre in the distorted dodecahedron with three O^{2-} ions being at distances that are long for coordination relative to those of Y^{3+}-O^{2-} in the perfect $Y_3Fe_5O_{12}$ crystal shown in Figure 3 (b). The Y^3 - Cr^{3+} distance gets reduced and the shortest Cr^{3+}-O^{2-} distances are found for the O^{2-} ions also coordinated to Y^{3+}. Since Y^{3+} is non-magnetic, its substitution on the octahedral site would enhance the magnetism. However, the presence of the magnetic Cr^{3+} ion on the 24c dodecahedral site would partly offset this increase as ions on this site would spin-align with those on the octahedral sites.

Figure 2 about here

Figure 3 about here

3.2. Defect structure of $Y_3Al_xCr_xFe_{5-2x}O_{12}$

The energies obtained for the defect reactions (*b.1-41*) for the Al^{3+} and Cr^{3+} co-doped $Y_3Fe_5O_{12}$ of the composition $Y_3Al_xCr_xFe_{5-2x}O_{12}$ are given in Table 4.

Table 4 about here

Examining these energy values, it is evident that defect reactions involving both of the Al^{3+} and Cr^{3+} ions occupying interstitial tetrahedral and/or octahedral sites (*b.*21-40) are unfavorable. Defect reactions with either of the substituted ions occupying interstitial sites and the other substituting Fe^{3+} at octahedral or tetrahedral sites (*b.*5-20) are also energetically unfavorable. Obviously the energetically favourable defect reactions are those where the Al^{3+} and/or Cr^{3+} ions simply substitute for Fe^{3+} ones (*b.*1-4) as well as the antisite defect reaction (*b.*41) where the Cr^{3+} ion substitutes for Y^{3+} at the dodecahedral sites and Al^{3+} substitutes for Fe^{3+} on a tetrahedral site with expelled Y^{3+} substituting for Fe^{3+} on an octahedral site. The defect model with the least energy is when both the Cr^{3+} and Al^{3+} ions substitute for Fe^{3+} at the tetrahedral sites (*b.*4). This reduces the contribution of the tetrahedral magnetic sub-lattice to the total magnetization and is, thus, consistent with the experimentally reported lower magnetization for $Y_3Al_xCr_xFe_{5-x}O_{12}$ relative to that of pure $Y_3Fe_5O_{12}$ [12-15].

However if we allow for the CFSE, as we did for $Y_3Cr_xFe_{5-x}O_{12}$, then the defect energy for the reaction in which Cr^{3+} substitutes for Fe^{3+} at an octahedral site and Al^{3+} substitutes for Fe^{3+} at a tetrahedral site (*b.*1) will be -3.94 eV whereas that for the reaction in which Cr^{3+}

substitutes for Fe^{3+} at a tetrahedral site and Al^{3+} substitutes for Fe^{3+} at an octahedral site (b.2) will be only -2.52 eV. It is, thus, evident that taking the CFSE into consideration renders the substitution of Cr^{3+} ion for octahedral Fe^{3+} ions and Al^{3+} at tetrahedral Fe^{3+} ions (b.1 in Table 4) to be the energetically most favorable defect structure for the co-substituted. Such a defect structure is consistent with the ab initio DFT calculations in that the Cr^{3+} preferentially substitutes at the octahedral sites. It also readily justifies observed reduction in the magnetization of the compound [12-15] relative to pure YIG as the nonmagnetic Al^{3+} ions reside in the magnetically dominant tetrahedral sub-lattice. One notes that in contrast with the cases discussed above when $Y_3Fe_5O_{12}$ structure is substituted with either Al^{3+} or Cr^{3+}, the inclusion of the CFSE in the case of the co-substitution makes the defect structure in which Cr^{3+} substitutes for octahedral Fe^{3+} and Al^{3+} substitutes for tetrahedral Fe^{3+}, (b.1), to be the most likely since its energy is distinctly lower than those of the other defect structures that involve substitution (b.2-4) as well as that of the antisite defect model (b.41). This, in turn, minimizes the effect of high temperature synthesis and/or the use of the initial reactants with undetected defects in yielding a different defect structure than that described in (b.1). To investigate the effect that co-substituting with Al^{3+} and Cr^{3+} will have on the lattice parameter, a 2×2×2 supercell of $Y_3Al_xCr_xFe_{5-2x}O_{12}$ containing Al^{3+} and Cr^{3+} in the tetrahedral and octahedral sites, respectively, was optimized. The calculated lattice parameter of that supercell was found to decrease relative to that of $Y_3Fe_5O_{12}$ in a trend similar to that reported experimentally [15] as is shown in Figure 4.

4 Conclusions

Interatomic potential calculations indicate that in Al^{3+}- substituted $Y_3Fe_5O_{12}$ the Al^{3+} ions preferentially substitute for Fe^{3+} at the tetrahedral sites leading to a reduced magnetisation relative to that of $Y_3Fe_5O_{12}$ as observed experimentally. The energy of this defect model was found to slightly lower than that of the model where the Al^{3+} ions substitute for octahedral Fe^{3+} ones suggesting that the latter model could also be possible for samples prepared under elevated temperatures and/or containing undetected point defects as, also, was proposed experimentally.
The CFSE and spin-spin coupling for Cr^{3+} ions were found to be decisive in showing the most favourable defect structure for $Y_3Cr_xFe_{5-x}O_{12}$ to be that in which the Cr^{3+} ions substitute for octahedral Fe^{3+} ions. The substitution of the Cr^{3+} for Y^{3+} ions that in turn substitute for Fe^{3+} ions at the octahedral sites was found to be possible particularly when undetected defects are present

and/or when high temperatures were used to prepare the material. This structural model, which results in distorted dodecahedrons with Cr^{3+} at off-centre positions, results in higher magnetization as has been experimentally reported. For the Al^{3+} and Cr^{3+}-co-substituted $Y_3Fe_5O_{12}$, the impurity Al^{3+} and Cr^{3+} ions were found to substitute for Fe^{3+} at the tetrahedral and octahedral sites respectively. The calculations suggest this defect structure to be stable regardless of the purity of the precursors or the processing conditions used.

Acknowledgement

References

[1] H. Hemme, H. Dötschm H. P. Menzler, Appl. Optics, 26 (1990), 3811

[2]. S. Geller, G.P. Espinosa, P.B. Crandall, J. Appl. Cryst. **2**, 86–88 (1969)

[3] Z. Cheng**,** H. Yang**,** L. Yu**,** Y. Cui**,** S. Feng, J. Mag. Mag. Mater., 320 (2006) 259

[4] H. M. Widatallah, C. Johnson, C., S. H. Al-Harthi, A. M. Gismelseed,A. D. Al-Rawas, S. J. Stewart, M. E. Elzain,I. A. Al-Omari, A. A. Yousif, Hyperfine Inter., 183 (2008) 87.

[5] M. Niyaifar , H. Mohammadpour, M. Dorafshani, A. Hasanpour, J. Magn. Magn. Mater., 409 (2016) 104.

[6] M. V. Kuznetsov, Q. A. Pankhurst, I. P. Parkin, L. Afflec, Y. G. Morozov, J. Mater. Chem., 10 (2000) 755.

[7] M. A. Gelleo, S. Geller, Phys. Rev., 110 (1958) 73

[8] C.S. Kim, B.K. Min, S.J. Kim, S.R. Yoon, Y.R. Uhm, J. Magn. Magn. Mater.*,* 245 (2003) 553.

[9] H. Donnerberg, C. R. A. Catlow, Phys. Rev. B, 50 (1994) 744.

[10] C. S. Kim, Y.K. Uhm, J-G Lee, K-H, Jeong, Mater. Sci. Forum, 373-376 (2001) 753.

[11] R. G. Burns, Geochimica et Cosmochimica Acta, 39 (1975) 857.

[12] V. D. Murumkar**,** K. B. Modi**,** K. M. Jadhav**,** G. K. Bichile**,** R. G. Kulkarni**,** Mater. Lett., 32 (1997), 281.

[13] V. D. Murumkar, D. R. Shengule, G. K. Bichile and K. M. Jadhav, Hyperfine Inter., 192-193 (2009) 100.

[14] A-F. Lahlooh, S. Mahmood, M. Mozaffari, J. Amighian, Hyperfine Inter. 156-157 (2004) 181.

[15] K. Bouziane, A. Yousif, H. M. Widatallah, J. Amighian, J. Mag. Mag. Mater., 320 (2008) 2330.

[16] M.J. Winter, www.webelements.com.

[17] C. V. Lewis, C. R. A. Catlow, J. Phys. C: Solid State Phys., 18 (1985) 1149.

[18] H. Donnerberg, C. R. A. Catlow, J. Phys.: Condens. Matter, 5 (1993) 2947.

[19] E. A. Moore, Annu. Rep. Prog. Chem. A, 104 (2008) 46.

[20] E. A. Moore, H.M. Widatallah, F. J. Berry, J. Phys. Chem. Solids, 63 (2002) 519

[21] M. M. Kuklja, J. Phys.: Condens. Matter, 12 (2000) 2953.

[22] H. M. Widatallah, E. A. Moore, A. A. Babu. M. S. Al Barwani, M. Elzain, Mater. Res. Bull., 43 (2012) 2361

[23] H. M. Widatallah, E. A. Moore, J. Phys., Chem. Solids, 65 (2004) 1663.

[24] E. A. Moore, H. M. Widatallah, Mater. Res. Bull., 43 (2008) 2361.

[25] N. L. Allan, W. C. Mackrodt, J. Chem. Soc., Faraday Trans., 86 (1990) 1227.

[26] J. Gale, J. Chem. Soc., Faraday Trans., 1 (1997) 629.

[27] R. Dovesi, R. Orlando, B. Civalleri, C. Roetti, V. R. Saunders, and C. M. Zicovich-Wilson, Z. Kristallogr. 220, 571 (2005).

[28] (a) A. D. Becke, J. Chem. Phys., **98**, 5648 (1993)

(b) S.H. Vosko, L. Wilk, M. Nusair, Can. J. Phys. 58 (1980) 1200.

[29] C. Lee, W. Yang and R. G. Parr, Phys. Rev. B, **37**, 785 (1988).

[30] http://www.tcm.phy.cam.ac.uk/~mdt26/crystal.html

[31] M. Catti, G. Valerio and R. Dovesi, Phys. Rev. B 51, 7441-7450 (1995).

[32] M. Catti, G. Valerio, R. Dovesi and M. Causa, Phys. Rev. B 49, 14179-14187 (1994).

[33] M Catti et al. J Phys Chem Solids 57 p. 1735 (1996)

[34] D. Rodic, M. Mitric, M.; R. Tellgren, H. Rundloef, A. Kremenovic, *J. of Mag. Mag.Mater*, 191 (1999) 137.

Table 1. Buckingham potential parameters, $V(r) = A \exp(-r/\rho) - Cr^{-6}$, spring constants and shell charge

Potential	A (eV)	ρ (Å)	C (eV Å^6)	Spring constant, k (eV Å^{-2})	Shell charge (e)
$Fe^{3+}_{(oct)}$shell –O^{2-} shell	993.9	0.3400	0.0		
$Fe^{3+}_{(tet)}$shell–O^{2-} shell	825.3	0.3490	0.0		
Y^{3+} corel–O^{2-}shell	1345.1	0.3491	0.0		
$Al^{3+}_{(oct)}$shell–O^{2-} shell	1114.9	0.3118	0.0		
$Al^{3+}_{(tet)}$shell–O^{2-}shell	1012.4	0.3118	0.0		
$Cr^{3+}_{(oct)}$shell–O^{2-}shell	1734.1	0.3010	0.0		
$Cr^{3+}_{(tet)}$shell–O^{2-}shell	1534.1	0.3010	0.0		
O^{2-} shell–O^{2-} shell	22764.0	0.1490	27.8	43.31	
$Fe^{3+}_{(oct)}$core– $Fe^{3+}_{(oct)}$ shell				408.0	5.30
$Fe^{3+}_{(tet)}$core– $Fe^{3+}_{(tet)}$ shell				205.0	4.65
Y^{3+}core– Y^{3+}shell				-	-
$Al^{3+}_{(oct)}$core– $Al^{3+}_{(oct)}$ shell				99999.0	3.000
$Al^{3+}_{(tet)}$core– $Al^{3+}_{(tet)}$ shell				99999.0	3.000
$Cr^{3+}_{(oct)}$core– $Cr^{3+}_{(oct)}$ shell				67.00	0.970
$Cr^{3+}_{(tet)}$core– $Cr^{3+}_{(tet)}$ shell				67.00	0.970
O^{2-}core– O^{2-}shell				43.31	-3.148

Table 2. Calculated lattice of α-Fe_2O_3, Al_2O_3 and Cr_2O_3 and defect energies in $Y_3Fe_5O_{12}$

Interaction	Lattice/Defect Energy(eV)
Fe_2O_3	-150.37012888
$V_{Fe(tet)}^{///}$	51.01484044
$V_{Fe(oct)}^{///}$	51.92532157
$V_O^{\bullet\bullet}$	21.45125838
Al_2O_3	-160.9214867
$Al_{Fe(tet)}$	-6.679663780
$Al_{Fe(oct)}$	-6.18962872
$Al_{int(tet)}^{\bullet\bullet\bullet}$	-47.18387648
$Al_{int(oct)}^{\bullet\bullet\bullet}$	-47.18387279
Cr_2O_3	-154.23548933
$Cr_{Fe(tet)}$	-4.51768175
$Cr_{Fe(oct)}$	-2.31695540
$Cr_{int(tet)}^{\bullet\bullet\bullet}$	-44.96227844
$Cr_{int(oct)}^{\bullet\bullet\bullet}$	-42.37978051
$Y_{Fe(oct)}$	1.51314509
Cr_Y	-12.22483744

Table 3 : Defect energies of the reactions for Al^{3+}-doped $Y_3Fe_5O_{12}$ and Cr^{3+}-doped $Y_3Fe_5O_{12}$.
(The brackets refer to the case of Cr^{3+}-doped $Y_3Fe_5O_{12}$).

Reaction no.	Process	Energy (eV)
a.1	Substitution of Al^{3+} (Cr^{3+}) for octahedral Fe^{3+}	-0.91; (-0.40)
a.2	Substitution of Al^{3+} (Cr^{3+}) for tetrahedral Fe^{3+}	-1.4; (-2.59)
a.3	Al^{3+} (Cr^{3+}) occupying an interstitial tetrahedral site balanced by a tetrahedral Fe^{3+} vacancy	9.10; (7.98)
a.4	Al^{3+} (Cr^{3+}) occupying an interstitial tetrahedral site balanced by an octahedral Fe^{3+} vacancy	10.01; (8.89)
a.5	Al^{3+} (Cr^{3+}) occupying an interstitial octahedral site balanced by an octahedral Fe^{3+} vacancy	10.0; (11.47)
a.6	Al^{3+} (Cr^{3+}) occupying an interstitial octahedral site balanced by a tetrahedral Fe^{3+} vacancy	9.1; (10.56)
a.7	Al^{3+} (Cr^{3+}) occupying an interstitial tetrahedral site balanced by equal numbers of tetrahedral and octahedral Fe^{3+} vacancies	9.56; (8.44)
a.8	Al^{3+} (Cr^{3+}) occupying an interstitial octahedral site balanced by equal numbers of octahedral and tetrahedral Fe^{3+} vacancies	9.56; (11.02)
a.9	Al^{3+} (Cr^{3+}) occupying an interstitial octahedral site with $3/2$ O^{-2} vacancies balanced by two octahedral Fe^{3+} vacancies.	18.93; (20.40)
a.10	Al^{3+} (Cr^{3+}) occupying an interstitial tetrahedral site with $3/2$ O^{-2} vacancies balanced by two octahedral Fe^{3+} vacancies.	18.93 (20.3)
a.11	Al^{3+} (Cr^{3+}) occupying an interstitial octahedral site with $3/2$ O^{-2} vacancies balanced by two tetrahedral Fe^{3+} vacancies.	17.1; (18.57)
a.12	Al^{3+} (Cr^{3+}) occupying an interstitial tetrahedral site with $3/2$ O^{-2} vacancies balanced by two tetrahedral Fe^{3+} vacancies.	17.1; (15.99)
a.13	Al^{3+} (Cr^{3+}) occupying an interstitial octahedral site with $3/2$ O^{-2} vacancies balanced by one octahedral vacancy and one tetrahedral Fe^{3+} vacancy.	18.0; (19.50)
a.14	Al^{3+} (Cr^{3+}) occupying an interstitial tetrahedral site with $3/2$ O^{-2} vacancies balanced by one octahedral vacancy and one tetrahedral Fe^{3+} vacancy.	17.99; (16.90)
a.15	$Al^{3+}(Cr^{3+})$ occupying an yttrium site with Y^{3+} substituting for Fe^{3+} on the nearest octahedral site	1.57;(-0.54)

Table 4 : Defect energies of the reactions for Al^{3+} and Cr^{3+}- co-substituted $Y_3Fe_5O_{12}$

Reaction no.	Process	Energy (eV)
b.1	Substitution of Cr^{3+} for an octahedral Fe^{3+} and Al^{3+} for a tetrahedral Fe^{3+}	-1.34
b.2	Substitution of Cr^{3+} for a tetrahedral Fe^{3+} and Al^{3+} for an octahedral Fe^{3+}	-1.75
b.3	Substitution of both Cr^{3+} and Al^{3+} for octahedral Fe^{3+} ions	-0.65
b.4	Substitution of both Cr^{3+} and Al^{3+} for tetrahedral Fe^{3+} ions	-1.99
b.5	Cr^{3+} occupying interstitial octahedral site and Al^{3+} substituting for tetrahedral Fe^{3+} balanced by an octahedral Fe^{3+} vacancy	5.04
b.6	Cr^{3+} occupying interstitial octahedral site and Al^{3+} substituting for octahedral Fe^{3+} balanced by an octahedral Fe^{3+} vacancy	5.28
b.7	Cr^{3+} occupying interstitial octahedral site and Al^{3+} substituting for tetrahedral Fe^{3+} balanced by a tetrahedral Fe^{3+} vacancy	4.58
b.8	Cr^{3+} occupying interstitial octahedral site and Al^{3+} substituting for octahedral Fe^{3+} balanced by a tetrahedral Fe^{3+} vacancy	4.83
b.9	Al^{3+} occupying interstitial octahedral site and Cr^{3+} substituting for tetrahedral Fe^{3+} balanced by an octahedral Fe^{3+} vacancy	3.72
b.10	Al^{3+} occupying interstitial octahedral site and Cr^{3+} substituting for octahedral Fe^{3+} balanced by an octahedral vacancy	4.82
b.11	Al^{3+} occupying interstitial octahedral site and Cr^{3+} substituting for tetrahedral Fe^{3+} balanced by a tetrahedral Fe^{3+} vacancy	3.26
b.12	Al^{3+} occupying interstitial octahedral site and Cr^{3+} substituting for octahedral Fe^{3+} balanced by a tetrahedral Fe^{3+} vacancy	4.36
b.13	Cr^{3+} occupying interstitial tetrahedral site and Al^{3+} substituting for tetrahedral Fe^{3+} balanced by an octahedral Fe^{3+} vacancy	3.75
b.14	Cr^{3+} occupying interstitial tetrahedral site and Al^{3+} substituting for octahedral Fe^{3+} balanced by an octahedral Fe^{3+} vacancy	3.99
b.15	Cr^{3+} occupying interstitial tetrahedral site and Al^{3+} substituting for tetrahedral Fe^{3+} balanced by a tetrahedral Fe^{3+} vacancy	3.29
b.16	Cr^{3+} occupying interstitial tetrahedral site and Al^{3+} substituting for octahedral Fe^{3+} balanced by a tetrahedral Fe^{3+} vacancy	3.54
b.17	Al^{3+} occupying interstitial tetrahedral site and Cr^{3+} substituting for tetrahedral Fe^{3+} balanced by an octahedral Fe^{3+} vacancy	3.72
b.18	Al^{3+} occupying interstitial tetrahedral site and Cr^{3+} substituting for octahedral Fe^{3+} balanced by an octahedral vacancy	4.82
b.19	Al^{3+} occupying interstitial tetrahedral site and Cr^{3+} substituting for tetrahedral Fe^{3+} balanced by a tetrahedral Fe^{3+} vacancy	3.26
b.20	Al^{3+} occupying interstitial tetrahedral site and Cr^{3+} substituting for octahedral Fe^{3+} balanced by a tetrahedral Fe^{3+} vacancy	4.36
b.21	Cr^{3+} and Al^{3+} occupying interstitial tetrahedral sites balanced by two tetrahedral Fe^{3+} vacancies	8.55
b.22	Cr^{3+} and Al^{3+} occupying interstitial tetrahedral sites balanced by two octahedral Fe^{3+} vacancies	9.46
b.23	Cr^{3+} and Al^{3+} occupying interstitial octahedral sites balanced by octahedral Fe^{3+} vacancies	10.75
b.24	Cr^{3+} and Al^{3+} occupying interstitial octahedral sites balanced by tetrahedral Fe^{3+} vacancies	9.84
b.25	Cr^{3+} and Al^{3+} occupying interstitial tetrahedral sites balanced by one octahedral and one tetrahedral Fe^{3+} vacancies	9.00

Table 4 (cont.) : Defect energies of the reactions for Al^{3+} and Cr^{3+}- co-

substituted $Y_3Fe_5O_{12}$

model	Process	Energy (eV)
b.26	Cr^{3+} and Al^{3+} occupying interstitial octahedral and interstitial tetrahedral sites, respectively, balanced by one octahedral and one tetrahedral Fe^{3+} vacancies.	10.29
b.27	Cr^{3+} and Al^{3+} occupying interstitial tetrahedral and octahedral sites, respectively, balanced by equal numbers of octahedral and tetrahedral Fe^{3+} vacancies.	10.29
b.28	Cr^{3+} and Al^{3+} occupying interstitial octahedral sites balanced by equal numbers of tetrahedral and octahedral Fe^{3+} vacancies.	10.29
b.29	For every Cr^{3+} and Al^{3+} and occupying interstitial octahedral sites three O^{2-} vacancies created balanced by four octahedral Fe^{3+} vacancies.	-19.67
b.30	For every Cr^{3+} and Al^{3+} and occupying interstitial octahedral sites three O^{2-} vacancies created balanced by four tetrahedral Fe^{3+} vacancies.	17.85
b.31	For every Cr^{3+} occupying an interstitial octahedral site and Al^{3+} occupying an interstitial tetrahedral sites three O^{2-} vacancies are created balanced by four octahedral Fe^{3+} vacancies.	19.67
b.32	For every Cr^{3+} occupying an interstitial octahedral site and Al^{3+} occupying an interstitial tetrahedral site three O^{2-} vacancies are created balanced by four tetrahedral Fe^{3+} vacancies.	17.85
b.33	For every Cr^{3+} occupying an interstitial tetrahedral site and Al^{3+} occupying an interstitial octahedral site three O^{2-} vacancies are created balanced by four octahedral Fe^{3+} vacancies.	18.38
b.34	For every Cr^{3+} occupying an interstitial tetrahedral site and Al^{3+} occupying an interstitial octahedral site three O^{2-} vacancies are created balanced by four tetrahedral Fe^{3+} vacancies.	16.55
b.35	For every Cr^{3+} and Al^{3+} and occupying interstitial tetrahedral sites three O^{2-} vacancies are created balanced by four octahedral Fe^{3+} vacancies.	18.38
b.36	For every Cr^{3+} and Al^{3+} and occupying interstitial tetrahedral sites three O^{2-} vacancies are created balanced by four tetrahedral Fe^{3+} vacancies.	16.55
b.37	For every Cr^{3+} and Al^{3+} and occupying interstitial octahedral sites three O^{2-} vacancies created balanced by two octahedral Fe^{3+} vacancies and two tetrahedral Fe^{3+} vacancies.	18.75
b.38	For every Cr^{3+} occupying an interstitial octahedral site and Al^{3+} occupying an interstitial tetrahedral site O^{2-} vacancies are created balanced by two octahedral Fe^{3+} vacancie and two tetrahedral Fe^{3+} vacancies.	18.75
b.39	For every Cr^{3+} occupying an interstitial tetrahedral site and Al^{3+} occupying an interstitial octahedral sites three O^{2-} vacancies are created balanced by two octahedral Fe^{3+} vacancies and one tetrahedral Fe^{3+} vacancies.	17.46
b.40	For every Cr^{3+} and Al^{3+} and occupying interstitial tetrahedral sites three O^{2-} vacancies are created balanced by two octahedral Fe^{3+} vacancies and two tetrahedral Fe^{3+} vacancies.	17.46
b.41	Cr^{3+} substituting for Y^{3+} and Al^{3+} substituting for Fe^{3+} on a tetrahedral site with Y^{3+} substituting for Fe^{3+} on an octahedral site.	-0.97

Figure captions:

Figure 1: The polyhedra of the O^{-2} ions (red small spheres) in the unit cell for cubic YIG. Both of the 4- and 6-O^{2-}coordinated tetrahedral (24 d) and octahedral (16a) sites of the Fe^{3+} ions (blue spheres) are shown in green whereas the 8-O^{2-}coordinated dodecahedral (24c) sites of the $Y^{3+ +}$ ions (orange large spheres) are shown in gray.

Figure 2: a) Environment of Y^{3+} on an O^{2-} octahedral (*a*) site. b) The corresponding environment of Fe^{3+} on an O^{2-} octahedron in in the perfect $Y_3Fe_5O_{12}$ crystal (*a*) site. Distances are in Å.

Figure 3: a) The distorted environment when an O^{2-} dodecahedron is occupied by Cr^{3+}. b) The corresponding environment of Y^{3+} on an O^{2-} dodecahedron site in the in the perfect $Y_3Fe_5O_{12}$ crystal. Distances are in Å.

Figure 4: a) The distorted environment when an O^{2-} dodecahedron is occupied by Cr^{3+}. b) The corresponding environment of Y^{3+} on an O^{2-} dodecahedron site in the in the perfect $Y_3Fe_5O_{12}$ crystal. Distances are in Å.